Appl. Math. Mech. -Engl. Ed., **34**(8), 1017–1030 (2013)
DOI 10.1007/s10483-013-1724-x

Applied Mathematics and Mechanics (English Edition)

2D numerical manifold method based on quartic uniform B-spline interpolation and its application in thin plate bending*

Wei-bin WEN (温伟斌)[1], Kai-lin JIAN (蹇开林)[1,2], Shao-ming LUO (骆少明)[3]

(1. School of Resources and Environmental Science, Chongqing University, Chongqing 400044, P. R. China;
2. State Key Laboratory of Coal Mine Disaster Dynamics and Control, Chongqing University, Chongqing 400044, P. R. China;
3. Faculty of Mechanical and Electrical Engineering, Zhongkai University of Agriculture and Engineering, Guangzhou 510225, P. R. China)

Abstract A new numerical manifold (NMM) method is derived on the basis of quartic uniform B-spline interpolation. The analysis shows that the new interpolation function possesses higher-order continuity and polynomial consistency compared with the conventional NMM. The stiffness matrix of the new element is well-conditioned. The proposed method is applied for the numerical example of thin plate bending. Based on the principle of minimum potential energy, the manifold matrices and equilibrium equation are deduced. Numerical results reveal that the NMM has high interpolation accuracy and rapid convergence for the global cover function and its higher-order partial derivatives.

Key words numerical manifold method (NMM), manifold element, B-spline, thin plate bending

Chinese Library Classification O302
2010 Mathematics Subject Classification 82-08, 82B05

1 Introduction

The numerical manifold method (NMM) based on topological manifold was originally proposed by Shi[1]. It combines the widely used finite element method (FEM) and the joint or block oriented discontinuous deformation analysis (DDA) in a unified form[2]. This method assimilates the advantages of the DDA and the FEM[2–3]. Based on the capabilities of the NMM in modeling continuous and discontinuous problems, various studies for the theory and application of the NMM were developed over the last few years. Most of the previous studies focused on the problems associated with rock failure[4] and crack propagation[5–8]. Recently, some researchers have successfully applied the NMM to other fields such as fatigue failure[9–10], seepage flow[11], and fluid field computation[12]. Present 2D manifold elements and 3D manifold elements mainly adopt the shape functions in the finite element analysis as their weight

* Received Aug. 27, 2012 / Revised Apr. 29, 2013
Project supported by the Fund of National Engineering and Research Center for Highways in Mountain Area (No. gsgzj-2012-05), the Fundamental Research Funds for the Central Universities of China (No. CDJXS12 24 00 03), and the Scientific Research Foundation of State Key Laboratory of Coal Mine Disaster Dynamics and Control (No. 2011DA105287-MS201213)
Corresponding author Kai-lin JIAN, Professor, Ph. D., E-mail: cqjian@cqu.deu.cn

functions, while the continuity and interpolation accuracy are uniformly enhanced by the use of different forms of basis functions for the local cover function[13–14]. It is noteworthy that the higher-order local cover functions related to global coordinates increase the condition number of stiffness matrices and even lead to ill-conditioned or singular equations. To enhance the quality of stiffness matrices and avoid the numerical instability caused by ill-conditioned matrices, Lin et al.[15] presented an improved local cover function that could effectively ameliorate the quality of stiffness matrices and enhance the stress precision. However, the number of the unknown degrees of freedom (DOFs) is still huge. Actually, for most conventional NMMs, increasing the polynomial order of local cover functions can induce the linear dependence (LD) among all shape functions of the manifold element, while the LD problem makes the rank of the stiffness matrix deficient and further causes failure in solving the ultimate equation[16–17]. In the conventional NMM, some problems that stem from the construction and generation of meshes cannot be ignored. In view of this consideration, Li and Cheng[18] studied the meshless numerical manifold method (MNMM) on the basis of the NMM and partition of unity (PU). By comparison with the conventional NMM, this method is more flexible in the selection of finite covers and can get rid of the disadvantages of the mesh in the NMM. The prepossession of the MNMM is simple. However, the above advantages are at the expense of low computational efficiency and dealing with a large number of nodes. Subsequently, the complex variable meshless manifold (CVMM) was put forward by Gao and Cheng[19]. This method can significantly reduce the number of nodes and is bound to improve computational efficiency. However, there is a lot of computation needed for the complex matrix inversion that to a great extent limits the further application of this method. Considering the disadvantages of the current manifold methods, this paper proposes a novel NMM with a concept of fixed uniform mesh. The new NMM utilizes the quartic uniform B-spline basis functions to construct the global cover function. The new manifold element possesses higher-order compatibility. The proposed NMM is applied for the numerical example of a thin plate bending to verify its calculation efficiency, and the concrete manifold formulations are also derived in this paper.

2 Fundamental theory of NMM

2.1 Basic concepts of NMM

The NMM employs two sets of separate and independent cover (mesh) systems, i.e., mathematical covers and physical covers. The mathematical covers that present small regions of the whole field can be arbitrarily selected regardless of shapes and sizes. The mathematical covers can be overlapped with each other either partially or totally and need not conform to physical covers. However, the total mathematical meshes should be large enough to cover the whole material volume. In contrast, the physical covers describe the geometry of the integration domain or the whole material volume. Hence, the selection of physical covers is not arbitrary and determined by material characteristics such as interior and exterior boundaries, cracks, voids, and interfaces of different material zones. In the finite cover system, overlapping the two meshes provides a manifold description. The intersection of the mathematical cover and the physical cover or the common region of the two systems defines the region of physical covers. A common area of the overlapped covers corresponds to an element in the manifold method. For convenience, the conventional NMM usually adopts finite element meshes or regular structures to generate mathematical covers and constructs the associated weight functions. The selection of suitable local cover functions and weight functions is very important for successful applications of the NMM. The global cover function is the weighted average of local cover functions on the common part of the associated covers (or manifold elements). Further details of geometrical aspects of the NMM were deliberately elucidated in the work of Shi[1].

2.2 Generation of global cover function

In the NMM, the cover weight functions are practically equivalent to the shape functions in the finite element analysis. The selected cover weight functions must satisfy the properties of the PU. The local cover function can be of various forms such as a constant basis function, a linear basis function, and a higher-order polynomial basis function. With regard to the 2D case, we denote the local cover function of any cover U_i as

$$u_i(x,y), \quad v_i(x,y), \quad (x,y) \in U_i. \tag{1}$$

The local cover function (u_i, v_i) in U_i can be constructed by a linear combination of mutually independent functions $f_{i,j}$ of a given order m and the constant coefficients $d_{i,2j-1}$ and $d_{i,2j}$. Therefore, Eq. (1) can be written in a matrix form as

$$\begin{bmatrix} u_i(x,y) \\ v_i(x,y) \end{bmatrix} = \sum_{j=1}^{m} \begin{bmatrix} f_{i,j}(x,y) & 0 \\ 0 & f_{i,j}(x,y) \end{bmatrix} \begin{bmatrix} d_{i,2j-1} \\ d_{i,2j} \end{bmatrix} = \boldsymbol{f}_i \boldsymbol{D}_i, \tag{2}$$

where $\boldsymbol{D}_i$ is called the local degree of the freedom vector.

Assume that any manifold element e presents the common part of several overlapped covers $U_{e(i)}\,(i = 1, 2, \cdots, q)$, and the function $N_{e(i)}(x,y)$ is the weight function corresponding to the cover $U_{e(i)}$. The displacement function (u, v) of the manifold element e can be approximated as

$$\begin{aligned} \begin{bmatrix} u(x,y) \\ v(x,y) \end{bmatrix} &= \sum_{i=1}^{q} N_{e(i)}(x,y) \begin{bmatrix} u_i(x,y) \\ v_i(x,y) \end{bmatrix} \\ &= \sum_{i=1}^{q} \sum_{j=1}^{m} \begin{bmatrix} N_{e(i)}(x,y) f_{e(i),j}(x,y) & 0 \\ 0 & N_{e(i)}(x,y) f_{e(i),j}(x,y) \end{bmatrix} \begin{bmatrix} d_{e(i),2j-1} \\ d_{e(i),2j} \end{bmatrix} \\ &= \sum_{i=1}^{q} N_{e(i)}(x,y) \boldsymbol{f}_i \boldsymbol{D}_{e(i)} = \boldsymbol{T}_e \boldsymbol{D}_e. \end{aligned} \tag{3}$$

3 2D manifold method with quartic uniform B-spline interpolation

3.1 Quartic uniform B-spline basis functions

There are a lot of ways to define the B-spline basis functions. We use a recurrence formula to define the B-spline basis functions since it is the most used one for computer implementation[20]. Let $\{x_1, x_2, \cdots, x_p\}$ be a nondecreasing sequence of real numbers, i.e., $x_i \leqslant x_{i+1}$ with $i = 0, 1, \cdots, p-1$. Here, x_i are called the B-spline knots. The ith B-spline function of k-degree, denoted by $B_{i,k}(x)$, is defined as

$$B_{i,0}(x) = \begin{cases} 1, & x_i \leqslant x < x_{i+1}, \\ 0, & \text{otherwise}, \end{cases} \tag{4}$$

$$B_{i,k}(x) = \frac{x - x_i}{x_{i+k} - x_i} B_{i,k-1}(x) + \frac{x_{i+k+1} - x}{x_{i+k+1} - x_{i+1}} B_{i+1,k-1}(x), \tag{5}$$

where the half-open interval $[x_i, x_{i+1})$ is called the ith B-spline knot span. Equation (5) can yield the quotient 0:0. We define this quotient to be zero.

$B_{i,k}(x) = 0$ if x is outside the interval $[x_i, x_{i+1})$ (the local support property). $B_{i,k}(x)$ is positive only for $x \in (x_i, x_{i+1})$. For an arbitrary B-spline knot span $[x_i, x_{i+1})$, the B-spline basis functions satisfy the PU for all $x \in [x_i, x_{i+1})$[21] as follows:

$$\sum_i B_{i,4}(x) = 1. \tag{6}$$

When all the B-spline knots are uniformly distributed, we can let $(x-x_i)/(x_{i+1}-x_i)=\xi_i$. By the definition of the B-spline basis function, the quartic uniform B-spline basis function can be expressed as

$$B_{i,4}(x)=\begin{cases}0, & x\notin[x_i,x_{i+5}],\\ \dfrac{1}{4!}\xi_i^4, & x\in[x_i,x_{i+1}],\\ \dfrac{1}{4!}(-4(\xi_i-1)^4+4(\xi_i-1)^3+6(\xi_i-1)^2+4(\xi_i-1)+1), & x\in[x_{i+1},x_{i+2}],\\ \dfrac{1}{4!}(6(\xi_i-2)^4-12(\xi_i-2)^3-6(\xi_i-2)^2+12(\xi_i-2)+11), & x\in[x_{i+2},x_{i+3}],\\ \dfrac{1}{4!}(-4(\xi_i-3)^4+12(\xi_i-3)^3-6(\xi_i-3)^2-12(\xi_i-3)+11), & x\in[x_{i+3},x_{i+4}],\\ \dfrac{1}{4!}(1-(\xi_i-4)^4), & x\in[x_{i+4},x_{i+5}].\end{cases}\tag{7}$$

3.2 2D manifold element with quartic uniform B-spline interpolation

Assume that (i,j) presents the rectangular element $[x_i,x_{i+1}]\times[y_j,y_{j+1}]$. Using the analogous method as the construction of B-spline surfaces, the global cover function of any given rectangular manifold element (i,j) can be written in a matrix form as

$$\begin{aligned}W_{i,j}(x,y)=&[B_{i-4,4}(x)\quad B_{i-3,4}(x)\quad B_{i-2,4}(x)\quad B_{i-1,4}(x)\quad B_{i-3,4}(x)]\\ &\cdot\begin{bmatrix}d_{i,j}&d_{i,j+1}&d_{i,j+2}&d_{i,j+3}&d_{i,j+4}\\ d_{i+1,j}&d_{i+1,j+1}&d_{i+1,j+2}&d_{i+1,j+3}&d_{i+1,j+4}\\ d_{i+2,j}&d_{i+2,j+1}&d_{i+2,j+2}&d_{i+2,j+3}&d_{i+2,j+4}\\ d_{i+3,j}&d_{i+3,j+1}&d_{i+3,j+2}&d_{i+3,j+3}&d_{i+3,j+4}\\ d_{i+4,j}&d_{i+4,j+1}&d_{i+4,j+2}&d_{i+4,j+3}&d_{i+4,j+4}\end{bmatrix}\begin{bmatrix}B_{j-4,4}(y)\\ B_{j-3,4}(y)\\ B_{j-2,4}(y)\\ B_{j-1,4}(y)\\ B_{j,4}(y)\end{bmatrix}\\ =&\sum_i\sum_j B_{i-4,4}(x)B_{j-4,4}(y)d_{i,j}=\boldsymbol{T}_{i,j}\boldsymbol{D}_{i,j},\end{aligned}\tag{8}$$

where $\boldsymbol{D}_{i,j}$ is the generalized displacement DOF vector of the manifold element (i,j), and $\boldsymbol{T}_{i,j}$ is called the generalized weight function corresponding to the manifold element (i,j). The concrete forms of $\boldsymbol{D}_{i,j}$ and $\boldsymbol{T}_{i,j}$ are

$$\boldsymbol{D}_{i,j}=[d_{i,j}\quad d_{i,j+1}\quad d_{i,j+2}\quad d_{i,j+3}\quad d_{i,j+4}\quad d_{i+1,j}\quad\cdots\quad d_{i+4,j+4}]^{\mathrm{T}},\tag{9}$$

$$\begin{aligned}\boldsymbol{T}_{i,j}=&[B_{i-4,4}(x)B_{j-4,4}(y)\quad B_{i-4,4}(x)B_{j-3,4}(y)\\ &B_{i-4,4}(x)B_{j-2,4}(y)\quad\cdots\quad B_{i+4,4}(x)B_{j+4,4}(y)].\end{aligned}\tag{10}$$

Assume that each entry of $\boldsymbol{T}_{i,j}$ is $(\boldsymbol{T}_{i,j})_k$. According to Eq. (6), we have the following relationship:

$$\sum_{k=1}^{25}(T_{i,j})_k=\sum_{k_1=0}^{4}B_{i-k_1,4}(x)\sum_{k_2=0}^{4}B_{i-k_2,4}(y)=1.\tag{11}$$

In other words, $\boldsymbol{T}_{i,j}$ satisfies the properties of the PU.

Based on the assumption of Eq. (7), for all $x \in (x_i, x_{i+1})$, the mathematical expressions of the quartic uniform B-spline functions can be given as

$$B_{i-4,4}(x) = \frac{1}{4!}(1-\xi_i)^4, \tag{12}$$

$$B_{i-3,4}(x) = \frac{1}{4!}(-4{\xi_i}^4 + 12{\xi_i}^3 - 6{\xi_i}^2 - 12\xi_i + 11), \tag{13}$$

$$B_{i-2,4}(x) = \frac{1}{4!}(6{\xi_i}^4 - 12{\xi_i}^3 - 6{\xi_i}^2 + 12\xi_i + 11), \tag{14}$$

$$B_{i-1,4}(x) = \frac{1}{4!}(-4{\xi_i}^4 + 4{\xi_i}^3 + 6{\xi_i}^2 + 4\xi_i + 1), \tag{15}$$

$$B_{i,4}(x) = \frac{1}{4!}(\xi_i)^4. \tag{16}$$

In the same way, we can obtain the quartic uniform B-spline functions for all $y \in (y_i, y_{i+1})$. The proposed B-spline basis functions are illustrated in Figs. 1 and 2. It can be observed that the quartic uniform B-spline functions have the terrific local support property that makes the generated global stiffness matrix symmetric. Meanwhile, all weight functions of any manifold element are linearly independent with each other. Therefore, the proposed B-spline basis functions can enhance the computational precision and efficiency greatly. According to the continuous property of quartic uniform B-spline basis functions[19], the proposed manifold element is C^3 compatible with respect to x and y, respectively.

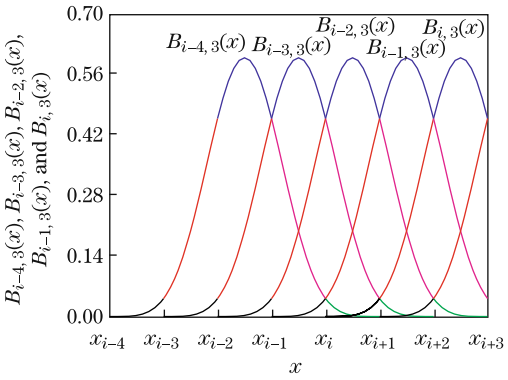

Fig. 1 Quartic uniform B-spline curve in piecewise form

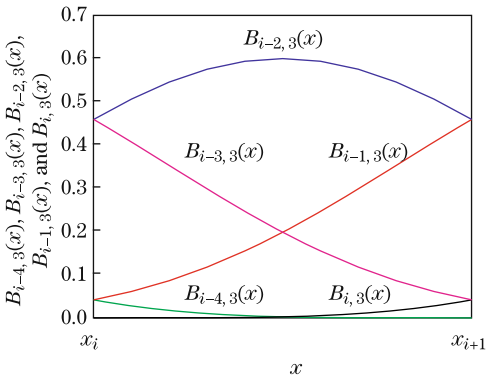

Fig. 2 Quartic uniform B-spline curve within element i

4 Analysis of thin plate bending with NMM

4.1 Strain energy with NMM

Assume that $W(x, y)$ is the displacement (deflection) function of thin plate bending, h is the thickness of the thin plate, E is Young's modulus (stress-strain) matrix, μ is Poisson's ratio, and Ω is the domain of integration. φ_x and φ_y are the rotation angles of a line, which are normal to the mid surface before the deformation about the x- and y-axes, respectively. κ_x and κ_y represent the bending curvatures in the x- and y-directions, respectively. κ_{xy} represents the twist curvature. ε_x, ε_y, and γ_{xy} are the stresses. M_x and M_y are the bending moments, and M_{xy} is the twisting moment. Q_x and Q_y are the shear forces. According to the Kirchhoff plate theory, the stresses and strains in the xz-plane and the yz-plane are negligible[22]. Thus, the

above physical variables can be rewritten in a column vector form as follows:

$$\boldsymbol{\varphi} = [\varphi_x \quad \varphi_y]^{\mathrm{T}}, \tag{17}$$

$$\boldsymbol{\varepsilon} = [\varepsilon_x \quad \varepsilon_y \quad \gamma_{xy}]^{\mathrm{T}}, \tag{18}$$

$$\boldsymbol{\kappa} = [\kappa_x \quad \kappa_y \quad \kappa_{xy}]^{\mathrm{T}}, \tag{19}$$

$$\boldsymbol{M} = [M_x \quad M_y \quad M_{xy}]^{\mathrm{T}}, \tag{20}$$

$$\boldsymbol{Q} = [Q_x \quad Q_y]^{\mathrm{T}}. \tag{21}$$

For small strains and small rotations, Eqs. (17)–(21) can be represented by the displacement function as

$$\boldsymbol{\varphi} = \boldsymbol{G}_1 W, \tag{22}$$

$$\boldsymbol{\kappa} = \boldsymbol{G}_2 W, \tag{23}$$

$$\boldsymbol{\varepsilon} = z\boldsymbol{\kappa} = z\boldsymbol{G}_2 W, \tag{24}$$

$$\boldsymbol{M} = \boldsymbol{D}_4\boldsymbol{\kappa} = \boldsymbol{D}_4\boldsymbol{G}_2 W, \tag{25}$$

$$\boldsymbol{Q} = \boldsymbol{G}_3\boldsymbol{M} = \boldsymbol{G}_3\boldsymbol{D}_4\boldsymbol{G}_2 W, \tag{26}$$

where

$$\boldsymbol{G}_1 = \left[\frac{\partial}{\partial x} \quad \frac{\partial}{\partial y}\right]^{\mathrm{T}}, \tag{27}$$

$$\boldsymbol{G}_2 = \left[-\frac{\partial^2}{\partial x^2} \quad -\frac{\partial^2}{\partial y^2} \quad -2\frac{\partial^2}{\partial x \partial y}\right]^{\mathrm{T}}, \tag{28}$$

$$\boldsymbol{G}_3 = \begin{bmatrix} \dfrac{\partial}{\partial x} & 0 & \dfrac{\partial}{\partial y} \\ 0 & \dfrac{\partial}{\partial y} & \dfrac{\partial}{\partial x} \end{bmatrix}, \tag{29}$$

$$\boldsymbol{D}_4 = \frac{Eh^3}{12(1-\mu^2)} \begin{bmatrix} 1 & \mu & 0 \\ \mu & 1 & 0 \\ 0 & 0 & (1-\mu)/2 \end{bmatrix}. \tag{30}$$

The strain energy stored in the thin plate can be expressed as

$$\prod\nolimits_U = \iint_{\Omega} \frac{1}{2}\boldsymbol{\kappa}^{\mathrm{T}}\boldsymbol{M}\mathrm{d}x\mathrm{d}y = \iint_{\Omega} \frac{1}{2}\boldsymbol{\kappa}^{\mathrm{T}}\boldsymbol{D}_4\boldsymbol{\kappa}\mathrm{d}x\mathrm{d}y. \tag{31}$$

Substituting Eqs. (23) and (25) into Eq. (31) can yield the following discrete form of the strain energy:

$$\begin{aligned} \prod\nolimits_U^* &= \sum_{i=1}^{N_1}\sum_{j=1}^{N_2} \iint_{\Omega_{i,j}} \frac{1}{2}\boldsymbol{\kappa}^{\mathrm{T}}\boldsymbol{D}_4\boldsymbol{\kappa}\mathrm{d}x\mathrm{d}y \\ &= \sum_{i=1}^{N_1}\sum_{j=1}^{N_2} \frac{1}{2}\boldsymbol{D}_{i,j}^{\mathrm{T}}\boldsymbol{K}_U^{(i,j)}\boldsymbol{D}_{i,j}, \end{aligned} \tag{32}$$

in which the subscripts i and j are the corresponding identities of the manifold elements, related to the x- and y-directions, respectively. $\boldsymbol{K}_U^{(i,j)}$ can be expressed as

$$K_U^{(i,j)} = \frac{1}{2}\iint_{\Omega_{i,j}} (\boldsymbol{G}_2\boldsymbol{T}_{i,j})^{\mathrm{T}}\boldsymbol{D}_4(\boldsymbol{G}_2\boldsymbol{T}_{i,j})\mathrm{d}x\mathrm{d}y. \tag{33}$$

For convenience, a new matrix $\boldsymbol{C}_{i,j}$ is introduced for the entire assembly of all element stiffness matrices. It can be defined by

$$\boldsymbol{D}_{i,j} = \boldsymbol{C}_{i,j}\boldsymbol{D}, \tag{34}$$

where $\boldsymbol{D}$ is the overall degree of the freedom vector.

In particular, for the proposed B-spline manifold element in Eq. (8), the matrix $\boldsymbol{C}_{i,j}$ can be explicitly expressed as

$$\boldsymbol{C}_{i,j} = \begin{bmatrix} \boldsymbol{0}_{5\times((i-1)(N_1+4)+j-1)} & \boldsymbol{I}_{5\times5} & \boldsymbol{0}_{5\times((N_1+4)(N_2+5-i)-j-4)} \\ \boldsymbol{0}_{5\times(i(N_1+4)+j-1)} & \boldsymbol{I}_{5\times5} & \boldsymbol{0}_{5\times((N_1+4)(N_2+4-i)-j-4)} \\ \boldsymbol{0}_{5\times((i+1)(N_1+4)+j-1)} & \boldsymbol{I}_{5\times5} & \boldsymbol{0}_{5\times((N_1+4)(N_2+3-i)-j-4)} \\ \boldsymbol{0}_{5\times((i+2)(N_1+4)+j-1)} & \boldsymbol{I}_{5\times5} & \boldsymbol{0}_{5\times((N_1+4)(N_2+2-i)-j-4)} \\ \boldsymbol{0}_{5\times((i+3)(N_1+4)+j-1)} & \boldsymbol{I}_{5\times5} & \boldsymbol{0}_{5\times((N_1+4)(N_2+1-i)-j-4)} \end{bmatrix}_{25\times((N_1+4)(N_2+4))}, \tag{35}$$

where the submatrix $\boldsymbol{I}_{5\times5}$ is the identity matrix of size 5×5. N_1 and N_2 are the corresponding numbers of the manifold elements, related to the x- and y-directions, respectively.

Substituting Eq. (34) into Eq. (32), we get

$$\prod\nolimits_U^* = \frac{1}{2}\boldsymbol{D}^{\mathrm{T}}\boldsymbol{K}_U\boldsymbol{D}, \tag{36}$$

where

$$\boldsymbol{K}_U = \sum_{i=1}^{N_1}\sum_{j=1}^{N_2}\boldsymbol{C}_{i,j}^{\mathrm{T}}\boldsymbol{K}_U^{(i,j)}\boldsymbol{C}_{i,j}. \tag{37}$$

4.2 Boundary conditions with NMM

It is assumed that n and s present the outward normal direction and the tangential direction of the material boundary, respectively. θ is the angle from the x-direction to the n-direction. φ_n, M_n, and Q_n present the rotation angle, the bending moment, and the shear force in the outward normal direction, respectively. M_{ns} is the twist moment. For the convenience of the following analysis, we let $l = \cos\theta$ and $m = \sin\theta$. Some matrices are introduced as follows:

$$\boldsymbol{A}_1 = [l \quad m], \tag{38}$$

$$\boldsymbol{A}_2 = [l^2 \quad m^2 \quad 2lm], \tag{39}$$

$$\boldsymbol{A}_3 = [-lm \quad lm \quad l^2 - m^2], \tag{40}$$

$$\boldsymbol{A}_4 = [-m \quad l]. \tag{41}$$

It can be easily verified that

$$\varphi_n = \boldsymbol{A}_1\boldsymbol{\varphi} = \boldsymbol{A}_1\boldsymbol{G}_1W, \tag{42}$$

$$Q_n = \boldsymbol{A}_1\boldsymbol{Q} = \boldsymbol{A}_1\boldsymbol{G}_3\boldsymbol{D}_4\boldsymbol{G}_2W, \tag{43}$$

$$M_n = \boldsymbol{A}_2\boldsymbol{M} = \boldsymbol{A}_2\boldsymbol{D}_4\boldsymbol{G}_2W, \tag{44}$$

$$M_{ns} = \boldsymbol{A}_3\boldsymbol{M} = \boldsymbol{A}_3\boldsymbol{D}_4\boldsymbol{G}_2W, \tag{45}$$

$$\frac{\partial M_{ns}}{\partial s} = \boldsymbol{A}_4\boldsymbol{G}_1M_{ns} = \boldsymbol{A}_4\boldsymbol{G}_1\boldsymbol{A}_3\boldsymbol{D}_4\boldsymbol{G}_2W. \tag{46}$$

With the higher-order continuity and compatibility of the proposed manifold element, all the essential boundary conditions can be explicitly or implicitly represented by the displacement function, and the displacement can be adopted as the only unknown variable. Herein, the

penalty method is used for the imposition of boundary conditions, and the generalized energy form corresponding to these boundary conditions can be expressed as

$$\begin{aligned}\prod\nolimits_{\mathrm{B}} =& \int_{S_1} \frac{1}{2}\beta_1(\varphi_n - \overline{\varphi}_n)^2 \mathrm{d}s + \int_{S_1+S_2} \frac{1}{2}\beta_2(W - \overline{W})^2 \mathrm{d}s + \int_{S_2+S_3} \frac{1}{2}\beta_3(M_n - \overline{M}_n)^2 \mathrm{d}s \\ &+ \int_{S_3} \frac{1}{2}\beta_4\Big(Q_n + \frac{\partial M_{ns}}{\partial s} - \overline{V}_n\Big)^2 \mathrm{d}s + \sum_{J_W} \frac{1}{2}\beta_5\big(W - \overline{W}\big)^2, \end{aligned} \tag{47}$$

where β_1, β_2, β_3, β_4, and β_5 are the given positive penalty parameters, S presents the whole boundary of the thin plate, S_1 is the clamped boundary, S_2 is the simply supported boundary, S_3 is the free boundary, J_W is the supported corner point with the prescribed displacement, $\overline{W}$ is the prescribed displacement, $\overline{\varphi}_n$ is the prescribed normal angle, $\overline{M}_n$ is the prescribed normal bending moment, and $\overline{V}_n$ is the prescribed transverse load (per unit length).

Substituting Eqs. (42)–(46) into Eq. (47) and applying Eqs. (8) and (34) can yield the discrete form of the generalized potential energy associated with the boundary conditions as follows:

$$\begin{aligned}\prod\nolimits_{\mathrm{B}}^{*} =& \sum_{i=1}^{N_1}\sum_{j=1}^{N_2} \frac{1}{2}\Big(\int_{S_1^{i,j}} \beta_1(\boldsymbol{H}_1^{(i,j)}\boldsymbol{D} - \overline{\varphi}_n)^{\mathrm{T}}(\boldsymbol{H}_1^{(i,j)}\boldsymbol{D} - \overline{\varphi}_n)\mathrm{d}s \\ &+ \int_{S_1^{i,j}+S_2^{i,j}} \beta_2(\boldsymbol{H}_2^{(i,j)}\boldsymbol{D} - \overline{W})^{\mathrm{T}}(\boldsymbol{H}_2^{(i,j)}\boldsymbol{D} - \overline{W})\mathrm{d}s \\ &+ \int_{S_2^{i,j}+S_3^{i,j}} \beta_3(\boldsymbol{H}_3^{(i,j)}\boldsymbol{D} - \overline{M}_n)^{\mathrm{T}}(\boldsymbol{H}_3^{(i,j)}\boldsymbol{D} - \overline{M}_n)\mathrm{d}s \\ &+ \int_{S_3^{i,j}} \beta_4(\boldsymbol{H}_4^{(i,j)}\boldsymbol{D} - \overline{V}_n)^{\mathrm{T}}(\boldsymbol{H}_4^{(i,j)}\boldsymbol{D} - \overline{V}_n)\mathrm{d}s \\ &+ \sum_{J_W} \beta_5(\boldsymbol{H}_2^{(i,j)}\boldsymbol{D} - \overline{W})^{\mathrm{T}}(\boldsymbol{H}_2^{(i,j)}\boldsymbol{D} - \overline{W})\Big), \end{aligned} \tag{48}$$

where

$$H_1^{(i,j)} = \boldsymbol{A}_1\boldsymbol{G}_1\boldsymbol{T}_{i,j}\boldsymbol{C}_{i,j}, \tag{49}$$

$$H_2^{(i,j)} = \boldsymbol{T}_{i,j}\boldsymbol{C}_{i,j}, \tag{50}$$

$$H_3^{(i,j)} = \boldsymbol{A}_2\boldsymbol{D}_4\boldsymbol{G}_2\boldsymbol{T}_{i,j}\boldsymbol{C}_{i,j}, \tag{51}$$

$$H_4^{(i,j)} = (\boldsymbol{A}_1\boldsymbol{G}_3\boldsymbol{A}_4\boldsymbol{G}_1\boldsymbol{A}_3)\boldsymbol{D}_4\boldsymbol{G}_2\boldsymbol{T}_{i,j}\boldsymbol{C}_{i,j}. \tag{52}$$

For convenience, Eq. (48) can be written in the simplified form as

$$\prod\nolimits_{\mathrm{B}}^{*} = \frac{1}{2}\boldsymbol{D}^{\mathrm{T}}\boldsymbol{K}_{\mathrm{B}}\boldsymbol{D} + \boldsymbol{D}^{\mathrm{T}}\boldsymbol{F}_{\mathrm{B}} + H_0, \tag{53}$$

where

$$\begin{aligned}\boldsymbol{K}_{\mathrm{B}}=&\sum_{i=1}^{N_1}\sum_{j=1}^{N_2}\Big(\beta_1\int_{S_1^{i,j}}(\boldsymbol{H}_1^{(i,j)})^{\mathrm{T}}\boldsymbol{H}_1^{(i,j)}\mathrm{d}s+\beta_2\int_{S_1^{i,j}+S_2^{i,j}}(\boldsymbol{H}_2^{(i,j)})^{\mathrm{T}}\boldsymbol{H}_2^{(i,j)}\mathrm{d}s\\&+\beta_3\int_{S_2^{i,j}+S_3^{i,j}}(\boldsymbol{H}_3^{(i,j)})^{\mathrm{T}}\boldsymbol{H}_3^{(i,j)}\mathrm{d}s+\int_{S_3^{i,j}}\beta_4(\boldsymbol{H}_4^{(i,j)})^{\mathrm{T}}\boldsymbol{H}_4^{(i,j)}\mathrm{d}s\\&+\sum_{J_W}\beta_5(\boldsymbol{H}_2^{(i,j)})^{T}(\boldsymbol{H}_2^{(i,j)})\Big),\end{aligned}\tag{54}$$

$$\begin{aligned}\boldsymbol{F}_{\mathrm{B}}=&\sum_{i=1}^{N_1}\sum_{j=1}^{N_2}\Big(\beta_1\int_{S_1^{i,j}}\overline{\varphi}_n(\boldsymbol{H}_1^{(i,j)})^{\mathrm{T}}\mathrm{d}s+\beta_2\int_{S_1^{i,j}+S_2^{i,j}}\overline{W}(\boldsymbol{H}_1^{(i,j)})^{\mathrm{T}}\mathrm{d}s\\&+\beta_3\int_{S_2^{i,j}+S_3^{i,j}}\overline{M}_n(\boldsymbol{H}_3^{(i,j)})^{\mathrm{T}}\mathrm{d}s+\beta_4\int_{S_3^{i,j}}\overline{V}_n(\boldsymbol{H}_4^{(i,j)})^{\mathrm{T}}\mathrm{d}s\\&+\sum_{J_W}\beta_5\overline{W}(\boldsymbol{H}_2^{(i,j)})^{\mathrm{T}}(\boldsymbol{H}_2^{(i,j)})\Big),\end{aligned}\tag{55}$$

$$\begin{aligned}H_0=&\sum_{i=1}^{N_1}\sum_{j=1}^{N_2}\frac{1}{2}\Big(\int_{S_1^{i,j}}\beta_1(\overline{\varphi}_n)^2\mathrm{d}s+\int_{S_1^{i,j}+S_2^{i,j}}\beta_2(\overline{W})^2\mathrm{d}s\\&+\int_{S_2^{i,j}+S_3^{i,j}}\beta_3(\overline{M}_n)^2\mathrm{d}s+\int_{S_3^{i,j}}\beta_4(\overline{V}_n)^2\mathrm{d}s+\sum_{J_W}\beta_5(\overline{W})^2\Big).\end{aligned}\tag{56}$$

4.3 Potential energy of loads with NMM

In the NMM, the natural boundary conditions for the tractions at the boundaries are satisfied by transferring the boundary tractions into the equivalent loads with respect to the generalized DOFs. It is assumed that the thin plate is subject to a laterally distributed load and a given concentrated force that are donated by q and P, respectively. The potential energy of the loads can be expressed as

$$\begin{aligned}\prod\nolimits_P=&\iint_\Omega -qW\mathrm{d}\Omega+\int_{S_2^{i,j}+S_3^{i,j}}\overline{M}_n\varphi_n\mathrm{d}s\\&-\int_{S_3^{i,j}}\overline{V}_nW\mathrm{d}s-\sum_{J_P}PW,\end{aligned}\tag{57}$$

where J_P is the position or point that the force P acted on.

Using Eqs. (8) and (34) in Eq. (57), we can obtain the following discrete form of Eq. (57):

$$\prod\nolimits_P^*=\boldsymbol{D}^{\mathrm{T}}\boldsymbol{F}_P,\tag{58}$$

where

$$\begin{aligned}F_P=&\sum_{i=1}^{N_1}\sum_{j=1}^{N_2}\Big(\iint_{\Omega_{i,j}}-q(\boldsymbol{T}_{i,j}\boldsymbol{C}_{i,j})^{\mathrm{T}}\mathrm{d}\Omega+\int_{S_2^{i,j}+S_3^{i,j}}\overline{M}_n(\boldsymbol{A}_1\boldsymbol{G}_1\boldsymbol{T}_{i,j}\boldsymbol{C}_{i,j})^{\mathrm{T}}\mathrm{d}s\\&+\int_{S_3^{i,j}}-\overline{V}_n(\boldsymbol{T}_{i,j}\boldsymbol{C}_{i,j})^{\mathrm{T}}\mathrm{d}s+\sum_{J_P}-P(\boldsymbol{T}_{i,j}\boldsymbol{C}_{i,j})^{\mathrm{T}}\Big).\end{aligned}\tag{59}$$

For simplicity, the total potential energy of the thin plate can be expressed as

$$\prod_G^* = \prod_U^* + \prod_{\mathrm{B}}^* + \prod_P^*. \tag{60}$$

By minimizing the total potential energy, we obtain the following equilibrium equation:

$$(\boldsymbol{K}_U + \boldsymbol{K}_{\mathrm{B}})\boldsymbol{D} = \boldsymbol{F}_{\mathrm{B}} + \boldsymbol{F}_P. \tag{61}$$

After solving $\boldsymbol{D}$, by Eqs. (34) and (8), the expression of the displacement function for any manifold element (i, j) can be expressed as

$$W = \boldsymbol{T}_{i,j}\boldsymbol{C}_{i,j}\boldsymbol{D}. \tag{62}$$

With the higher-order continuation and compatibility of the displacement function, its partial derivatives can be derived by the direct displacement derivation. For the polynomial cover function, the Gauss integration scheme can be adopted for the rectangular integration domain, and the Hammer or simplex integration scheme can be adopted for the irregular integration domain that is divided into different triangulars[1,14].

5 Numerical example and analysis

5.1 Bending of thin plate with simply supported boundaries

A rectangular thin plate with four simply supported boundaries is shown in Fig. 3. The dimensions and parameters used for the analysis are $a = 6\,\mathrm{m}$, $b = 4\,\mathrm{m}$, the thickness of the thin plate $h = 1 \times 10^{-2}\,\mathrm{m}$, the lateral distributed load $q = 10\,\mathrm{kPa}$, Yong's modulus $E = 210\,\mathrm{GPa}$, Poisson's ratio $\mu = 0.3$, and the penalty parameter $\beta = 1.0 \times 10^9$. As depicted in Fig. 4, the fixed-mesh mathematical covers are adopted, and the proposed rectangular mathematical covers are big enough to cover the whole physical meshes. The divided shade region is a manifold element. For the proposed numerical example, the theoretical solution of the displacement field can be finally calculated as

$$W(x, y) = \sum_{i=1,3,5,\cdots} \sum_{j=1,3,5,\cdots} \frac{16q}{ij\pi^6 D_0 \left(\frac{i^2}{a^2} + \frac{j^2}{b^2}\right)^2} \sin\frac{i\pi x}{a} \sin\frac{j\pi y}{b}, \tag{63}$$

where $D_0 = \frac{Eh^3}{12(1-\mu^2)}$ is the bending rigidity of the thin plate.

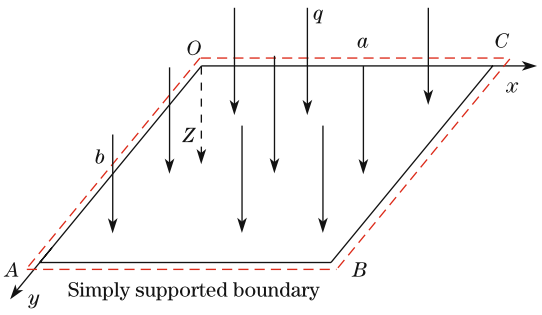

Fig. 3 Scheme and configuration of rectangular thin plate bending

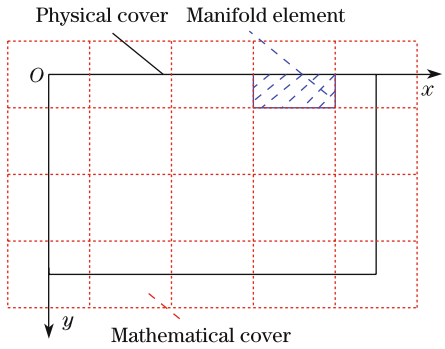

Fig. 4 Mathematical covers and manifold elements of rectangular thin plate

5.2 Analysis of numerical results

The numerical results obtained from the proposed NMM are compared with the theoretical solutions given in Eq. (63) in the following analysis. As listed in Table 1, at a given measure point $x = a/3$, $y = b/3$, the numerical results and theoretical solutions of the displacement and its several partial derivatives are given, and the relative error is used to indicate the accuracy of the numerical calculation. In Table 1, the relative error of the numerical displacement W', denoted by η, is defined as $\eta = \frac{|W'-W|}{|W|} \times 100\%$. Let $W_{,ij} = \frac{\partial^{(i+j)}W}{\partial x^i \partial y^j}$ be the theoretical solution of any partial derivative of the displacement and $W'_{,ij}$ be the corresponding numerical solution. As shown in Tables 1 and 2, we assume that $\eta_{,ij}$ is the relative error of $W'_{,ij}$. Thus, we define $\eta_{,ij}$ as $\eta_{,ij} = \frac{|W'_{,ij}-W_{,ij}|}{|W_{,ij}|} \times 100\%$. In Tables 1 and 2, various meshes are investigated to test the convergence of the proposed method. It can be obviously seen that the errors of the calculated displacement and its partial derivatives decrease rapidly as the element number increases. When the element number increases to 9×9, the relative error of the displacement W' falls to 0.005%, and the numerical result of the higher-order partial derivative $W'_{,22}$ is only 0.047% away from the theoretical solution. Actually, with the further increase of the element number, we can obtain more accurate numerical results.

Table 1 Displacement and its low-order partial derivatives at given point $x = a/3, y = b/3$

Element	$W'_{,ij}$							
	W'/m	η/%	$W'_{,11}$	$\eta_{,11}$/%	$W'_{,20}$	$\eta_{,20}$/%	$W'_{,02}$	$\eta_{,02}$/%
2×2	0.797 52	0.530 0	0.104 421	13.880 0	–0.217 50	4.530	–0.489 38	0.890 0
3×3	0.796 08	0.240 0	0.091 475	0.240 0	–0.217 11	4.340	–0.488 49	0.710 0
4×4	0.794 28	0.016 0	0.092 167	0.520 0	–0.206 64	0.690	–0.484 01	0.210 0
5×5	0.794 11	0.005 0	0.091 847	0.170 0	–0.207 52	0.270	–0.485 41	0.076 0
7×7	0.794 18	0.003 8	0.091 646	0.052 0	–0.207 79	0.140	–0.484 89	0.031 0
9×9	0.794 19	0.005 0	0.091 689	0.005 5	–0.208 17	0.043	–0.485 08	0.008 2
$W_{,ij}$	0.794 15	0.000 0	0.091 694	0.000 0	–0.208 08	0.000	–0.485 04	0.000 0

Table 2 Higher-order derivatives of displacement at given point $x = a/3$, $y = b/3$

Element	$W'_{,ij}$					
	$W'_{,12}$	$\eta_{,12}$/%	$W'_{,21}$	$\eta_{,21}$/%	$W'_{,22}$	$\eta_{,22}$/%
2×2	–0.144 58	14.710 0	0.096 39	4.360	0.133 46	20.000
3×3	–0.123 00	2.410 0	0.094 01	1.790	0.133 22	4.000
4×4	–0.125 59	0.360 0	0.090 99	1.480	0.126 52	1.230
5×5	–0.126 32	0.220 0	0.093 47	1.200	0.130 54	1.900
7×7	–0.125 95	0.071 0	0.092 08	0.300	0.127 73	0.290
9×9	–0.126 05	0.007 9	0.092 39	0.032	0.128 16	0.047
$W_{,ij}$	–0.126 04	0.000 0	0.092 36	0.000	0.128 10	0.000

In Fig. 5, the numerical results of the displacement and its partial derivatives are plotted along the direction of $x = a/3$. As illustrated in Fig. 5(a), we can acquire very accurate numerical displacement with only 4×4 elements. By contrast, for the partial derivatives, we need to adopt more elements to obtain the highly accurate numerical results (see Figs. 5(b)–5(g)). In Tables 1 and 2 and Fig. 5, only a given measure point or a series of measure points in a given direction are considered. Thus, it cannot fully indicate the global error within the whole thin plate. To indicate the global error of the numerical calculation, a new error norm of the displacement W', denoted by δ, is defined as $\delta = \frac{\sqrt{\sum_{k=1}^{N_a}(W'-W)^2}}{\sqrt{\sum_{k=1}^{N_a}(W')^2}} \times 100\%$, where N_a is the

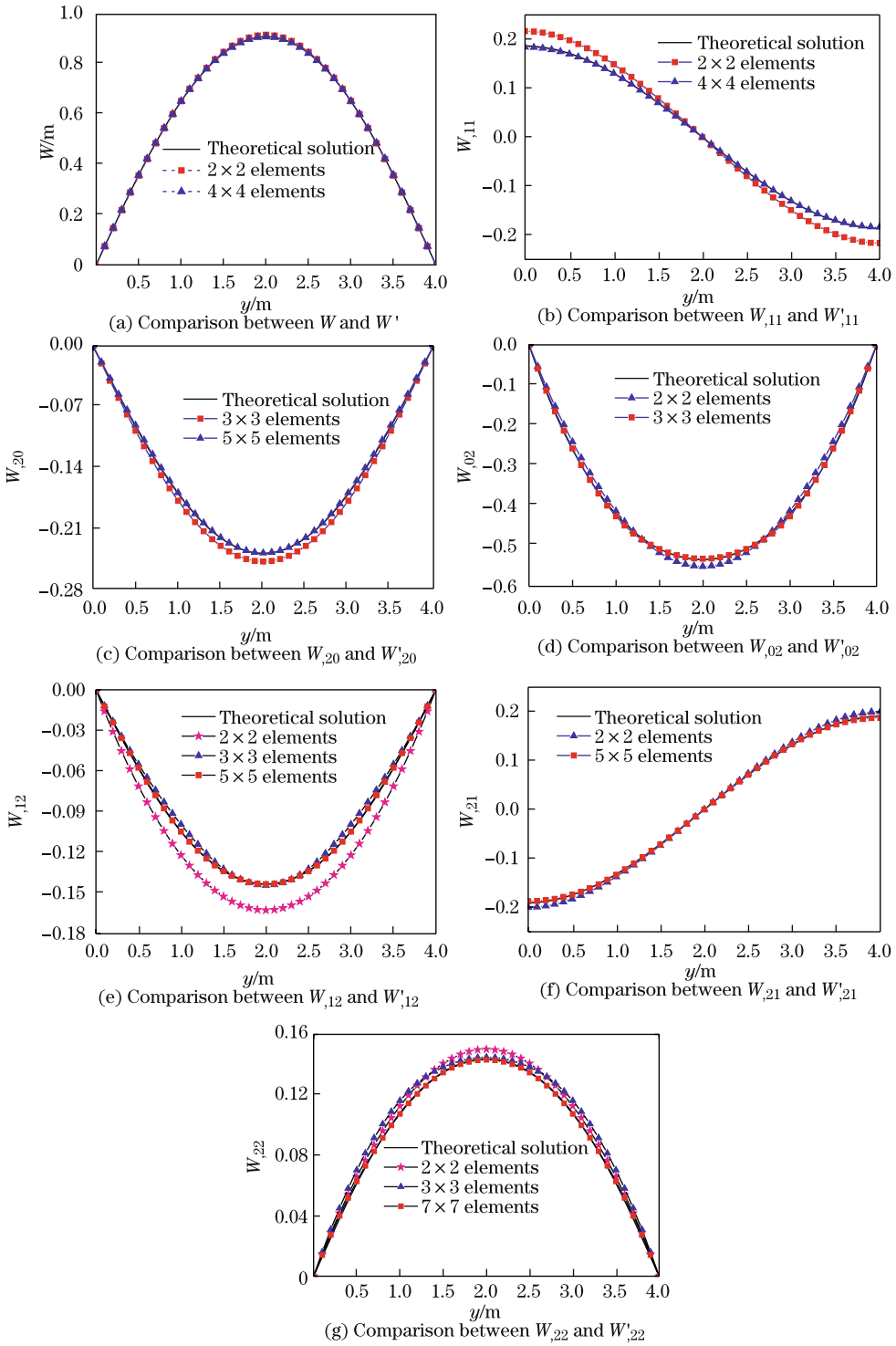

Fig. 5 Displacement and its partial derivatives of thin plate bending along direction of $x = a/3$

number of the measure points that are uniformly distributed along the x- and y-directions, respectively. As listed in Table 3, we denote that $\delta_{,ij}$ is the global error of $W'_{,ij}$. Then, we

define it in the same way as δ. For the proposed numerical example, we select $N_a = 21 \times 21$ within the whole thin plate. As enumerated in Table 3, when the element number increases, the global errors of the displacement and its partial derivatives rapidly decrease. As shown in Table 3, when the element number increases to 9×9, the global error of the displacement W' falls to 0.007 9%, and the global errors of the partial derivatives are relatively large, especially for the higher-order mixed partial derivative $\delta_{,22}$. To obtain more desirable results of the partial derivatives, we need to further increase the number of the elements.

The above numerical verification demonstrates that the results obtained from the proposed NMM agree well with the theoretical solutions, and thus reveals the validity of the given method for the numerical calculation.

Table 3 Global errors of displacement and its partial derivatives

Element	$\delta_{,ij}/\%$						
	δ_0	$\delta_{,20}$	$\delta_{,11}$	$\delta_{,02}$	$\delta_{,21}$	$\delta_{,12}$	$\delta_{,22}$
2×2	2.390 0	21.73	7.63	3.760	22.59	8.99	26.10
3×3	0.260 0	6.69	1.61	0.990	7.76	2.97	13.15
4×4	0.094 0	3.26	0.84	0.440	4.53	2.12	10.52
5×5	0.027 0	1.65	0.42	0.220	2.70	1.30	7.58
7×7	0.007 9	0.57	0.20	0.075	1.28	0.75	4.63
9×9	0.007 3	0.27	0.14	0.055	0.72	0.59	3.00

6 Conclusions

Based on the quartic uniform B-spline interpolation, a new 2D NMM is proposed in the present paper. The analysis shows that the new manifold element has a simple structure and possesses the higher-order continuation and polynomial consistency. The local support property of the quartic uniform B-spline function makes the calculated global stiffness matrix with good quality and overcomes the LD problem in the conventional NMM. Thus, it can enhance the calculation accuracy and efficiency greatly. With the higher-order compatibility of the proposed element, the proposed NMM is applied for the analysis of thin plate bending. The unified manifold formulations for the thin plate subject to different loads and boundary conditions are derived on the basis of the theorem of minimum potential energy. The numerical results demonstrate that the proposed NMM has high interpolation accuracy for the global cover function and its higher-order partial derivatives. The calculated results are in good agreement with the theoretical solutions.

Acknowledgements We are grateful to the referees for their valuable suggestions.

References

[1] Shi, G. H. Manifold method of material analysis. *Transactions of the 9th Army Conference of Applied Mathematics and Computing*, Minneapolis, Minnesota, 57–76 (1991)

[2] Ma, G. W., An, X. M., and He, Li. The numerical manifold method: a review. *International Journal of Computational Methods*, **7**(1), 1–32 (2010)

[3] Li, S., Cheng, Y., and Wu, Y. F. Numerical manifold method based on the method of weighted residuals. *Computational Mechanics*, **35**(6), 470–480 (2005)

[4] Li, S. C. and Cheng, Y. M. Numerical manifold method and its applications in rock mechanics (in Chinese). *Advances in Mechanics*, **34**(6), 446–454 (2004)

[5] Zhang, G. X., Zhao, Y., and Peng, X. C. Simulation of toppling failure of rock slope by numerical manifold method. *International Journal of Computational Methods*, **7**(1), 167–189 (2010)

[6] Zhang, H. H., Li, L. X., and An, X. M. Numerical analysis of 2D crack propagation problems using the numerical manifold method. *Engineering Analysis with Boundary Elements*, **34**(1), 41–50 (2010)

[7] Wu, Z. J. and Wong, L. N. Y. Frictional crack initiation and propogation analysis using the numerical manifold method. *Computers and Geotechnics*, **39**, 38–53 (2012)

[8] Li, S. C., Li, S. C., and Cheng, Y. M. Enriched meshless manifold method for two-dimensional crack modeling. *Theoretical and Applied Fracture Mechanics*, **44**(3), 234–248 (2005)

[9] Kourepinis, D., Pearce, C., and Bicanic, N. Higher-order discontinuous modeling of fracturing in concrete using the numerical manifold method. *International Journal of Computational Methods*, **7**(1), 83–106 (2010)

[10] Gao, H. F. and Cheng, Y. M. A complex variable meshless manifold method for fracture problems. *International Journal of Computational Methods*, **7**(1), 55–81 (2010)

[11] Jiang, Q. H., Deng, S. S., Zhou, C. B., and Lu, W. B. Modeling unconfined seepage flow using three-dimensional numerical manifold method. *Journal of Hydrodynamics*, **22**(4), 554–561 (2010)

[12] Zhang, Z. R., Zhang, X. W., and Yan, J. H. Manifold method coupled velocity and pressure for Navier-Stokes equations and direct numerical solution of unsteady incompressible viscous flow. *Computers and Fluids*, **39**(8), 1353–1365 (2010)

[13] Song, J. S. and Ohnishi, Y. High order rectangular element of manifold method (in Chinese). *Chinese Journal of Rock Mechanics and Engineering*, **22**(6), 932–936 (2003)

[14] Luo, S. M., Zhang, X. W., Lv, W. G., and Jiang, D. R. Theoretical study of three-dimensional numerical manifold method. *Applied Mathematics and Mechanics* (*English Edition*), **26**(9), 1027–1032 (2005) DOI 10.1007/BF02507721

[15] Lin, S. Z., Qi, Y. F., and Su, H. D. Improved local function of numerical manifold method and its application (in Chinese). *Journal of Yangtze River Scientific Research Institute*, **23**(6), 55–58 (2006)

[16] Taylor, R. L., Zienkiewicz, O. C., and Onate, E. A hierarchical finite element method based on partition of unity. *Computer Methods in Applied Mechanics and Engineering*, **152**(1-2), 73–84 (1998)

[17] Cai, Y. C., Zhuang, X. Y., and Augarde, C. A new partition of unity finite element free from the linear dependence problem and possessing the delta property. *Computer Methods in Applied Mechanics and Engineering*, **199**(17-20), 1036–1043 (2010)

[18] Li, S. C. and Cheng, Y. M. Meshless numerical manifold method based on unity partition (in Chinese). *Chinese Journal of Theoretical and Applied Mechanics*, **36**(4), 496–500 (2004)

[19] Gao, H. F. and Cheng, Y. M. Complex variable numerical manifold method for elasticity (in Chinese). *Chinese Journal of Theoretical and Applied Mechanics*, **41**(4), 480–488 (2009)

[20] Sevilla, R., Fernandez-Mendez, S., and Huerta, A. NURBS-enhanced finite element method (NEFEM). *Archives of Computational Methods in Engineering*, **18**(4), 441–484 (2011)

[21] Piegl, L. and Tiller, W. *The NURBS Book*, 2nd ed., Springer, London, 81–110 (1996)

[22] Barber, J. R. *Elasticity*, 2nd ed., Klüwer Academic Publishers, New York, 33–39 (2004)